LAWRENCE
LIVERMORE
NATIONAL
LABORATORY

UCRL-JRNL-225079

Ideal Laser Beam Propagation through high temperature ignition hohlraum plasmas

D. H. Froula, L. Divol, N. Meezan, S. Dixit, J. D. Moody, B. B. Pollock, J. S. Ross, S. H. Glenzer

October 7, 2006

Physical Review Letters

Ideal laser beam propagation through high temperature ignition hohlraum plasmas

D. H. Froula,* L. Divol, N. B. Meezan, S. Dixit, J. D. Moody, B. B. Pollock,† J. S. Ross, and S. H. Glenzer

L-399, Lawrence Livermore National Laboratory,

P.O. Box 808, Livermore, CA 94551, USA

(Dated: October 3, 2006)

Abstract

We demonstrate that a blue (3ω, 351 nm) laser beam with an intensity of 2×10^{15} W-cm^{-2} propagates within the original beam cone through a 2-mm long, T_e=3.5 keV high density ($n_e = 5 \times 10^{20}$ cm^{-3}) plasma. The beam produced less than 1% total backscatter; the resulting transmission is greater than 90%. Scaling of the electron temperature in the plasma shows that the plasma becomes transparent for uniform electron temperatures above 3 keV. These results are consistent with linear theory thresholds for both filamentation and backscatter instabilities inferred from detailed hydrodynamic simulations. This provides a strong justification for current inertial confinement fusion designs to remain below these thresholds.

PACS numbers: 52.25.Os, 52.35.Fp, 52.50.Jm

*Electronic address: froula1@llnl.gov

†Also at Engineering Department, University of Pacific, 3601 Pacific Avenue, Stockton, CA 95211

Inertial confinement fusion and high energy density science experiments at large laser facilities require efficient laser beam propagation through long under-dense plasmas to deposit energy at a desired region of interest. In the indirect drive approach to inertial confinement fusion (ICF), a high-Z radiation cavity (hohlraum) filled with a low density gas is used to convert laser energy into soft x-ray radiation to drive a fusion capsule implosion by ablation pressure [1]. For achieving a symmetric capsule implosion and for reaching ignition conditions, it is required that the energetic laser beams efficiently propagate through the interior of the hohlraum and create soft x rays close to where the laser beams were initially pointed on the hohlraum wall. The inside of the hohlraum will be filled with a low-Z or mid-Z long-scale length ($L \sim 2-4$ mm), high-temperature ($T_e \gg 3$ keV) plasma ranging in density from $n_e = 5 \times 10^{20}$ to $n_e = 15 \times 10^{20}$ cm^{-3} consisting of the initial fill material, ablated material off the capsule, and other lined hohlraum surfaces. The physics of laser beam propagation in ignition hohlraums is largely dominated by the laser-plasma interactions in the fill plasma where laser backscattering, beam deflection, beam filamentation, and self focusing may occur when driving these instabilities beyond their thresholds [2].

In this study, we present experiments that for the first time demonstrate transparent plasmas in high electron temperature ignition conditions. A 3ω (351 nm) laser beam with an intensity of 2×10^{15} W-cm^{-2} propagates within the original beam cone through a 2-mm long, T$_e$=3.5 keV, under-dense (n$_e$ = 5×10^{20} cm^{-3}) plasma. We show that increasing the electron temperature reduces the total backscatter. At a peak electron temperature of 3.5 keV, less than 1% total backscatter and a transmission greater than 90% is observed. The plasma conditions have been well-characterized using Thomson scattering and the electron temperature is controlled by varying the total laser energy used to heat the target [3]. It is shown that reducing the electron temperature or increasing the intensity of the laser beam reduces the threshold for filamentation and stimulated Brillouin scatter (SBS).

A new target platform (Fig. 1a) for studying laser-plasma interactions in 2-mm long high temperature plasmas has been developed by aligning an interaction beam down the axis of a gas-filled gold cylinder (hohlraum); this allows direct measurements of the laser beam propagation and transmission through ignition hohlraum plasmas. The hohlraum is heated by thirty-three frequency tripled (λ = 351 nm) laser beams at the Omega Laser Facility [4]. The electron temperature along the interaction beam path is controlled by varying the heater beam energy from a maximum of 17 kJ; the plasma conditions along the

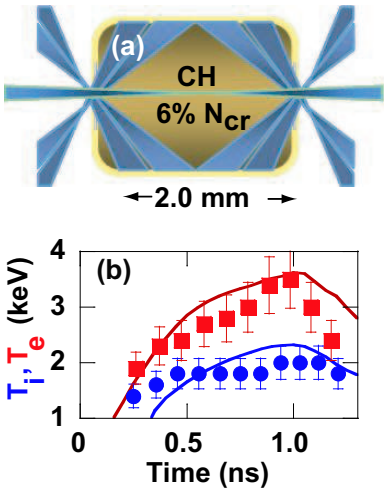

FIG. 1: A 3ω interaction beam with a maximum power averaged intensity of 4×10^{15} W-cm^{-2} is aligned along the axis of a gas-filled hohlraum where 33 heater beams heat the CH gas to a maximum electron temperature of 3.5 keV. (b) The electron temperature at the center of the hohlraum is measured using Thomson scattering where the total heater beam energy has been scaled from 8 kJ (circles) to 17 kJ (squares); the measurements are reproduced by hydrodynamic simulations (curves).

interaction beam path have been measured using Thomson scattering (Fig. 1b) validating 2-dimensional HYDRA [5] hydrodynamic simulations that show a uniform 1.6-mm plasma with a peak electron temperature of 3.5 keV [3]. These results provide confidence in the hydrodynamic parameters used as the foundation for laser plasma interaction modeling. The interaction experiments are performed in the uniform density plateau and before the shock waves driven by laser beam ablation at the gold wall reach the hohlraum axis, t $\simeq$ 1.3ns (stagnation)[6].

This new target platform together with recently commissioned suite of laser-plasma interaction diagnostics [7, 8] allows the access to high temperature, long scale length conditions not previously available using gasbag [9, 10], toroidal hohlraum [11, 12], or gas-filled hohlraum targets. Laser-plasma interaction thresholds are sensitive to the electron temperature and the length of the density plateau in a plasma; electron temperatures in open geometry gasbag plasmas with roughly the same plasma conditions are significantly lower than the target platform presented while scale lengths were much shorter in previous hohlraum platforms.

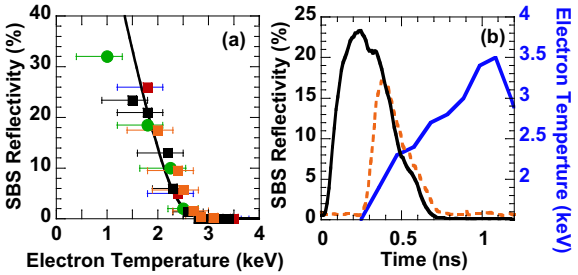

FIG. 2: (a) The SBS reflectivity is significantly reduced as the electron temperature is increased for an intensity of $I_p = 1.7 \times 10^{15}$ W-cm^{-2}. The instantaneous reflectivities are obtained by time resolving the backscatter and varying the total heater beam energy from 8 kJ (circles) to 16 kJ (squares). Each point represents an average over 200 ps and each color corresponds to a separate shot. (b) By delaying the interaction beam by 200 ps (dashed orange line) the beam interacts primarily with hot plasma thus reducing the total (time-averaged) and peak SBS. As the electron temperature reaches 2.5 keV (solid blue, right axis), the total backscatter goes to zero.

Gold 1.6-mm diameter, 2-mm long hohlraum targets produce a uniform density plateau using 1 atm of gas fill consisting of 30% CH_4, and 70% C_3H_8 expressed as partial pressures. The heater beams (1 ns square pulse) are focused near the 800 micron diameter laser entrance holes. The plasma conditions along the interaction beam path (T_e = 3.5 keV, $n_e = 5 \times 10^{20}$ cm^{-3}, L = 1.6 mm) are comparable to the scale lengths before the ablation region on current ignition targets planned to be shot on the NIF ($T_e > 3.0$ keV, $n_e \simeq 5 \times 10^{20}$ cm^{-3}, L $\simeq$ 2.0 mm).

The 3ω interaction beam (1 ns square pulse) is focused by a f/6.7 lens through a continuous phase plate (CPP) to a minimum vacuum diameter at the center of the hohlraum of 100 microns. The power averaged intensity at best focus for this beam is $I_p = 8.5 \times 10^{12}$E[J], where E is the incident laser beam energy ranging from 100 J to 400 J.

Light scattered from the interaction beam is measured using a full-aperture backscatter station (FABS), near backscatter imager (NBI), and a 3ω transmitted beam diagnostic (3ωTBD) [8]. Light scattered back into the original beam cone is collected by the FABS; both the SBS (351 nm) and SRS (500 nm) spectrum and energy are independently measured. Backscattered light outside of the original beam cone reflects from a plate surrounding the interaction beam. The plate is imaged onto two charge-coupled devices (CCD) which time integrate the SBS and SRS signals. The 3ωTBD allows us to accurately measure the light

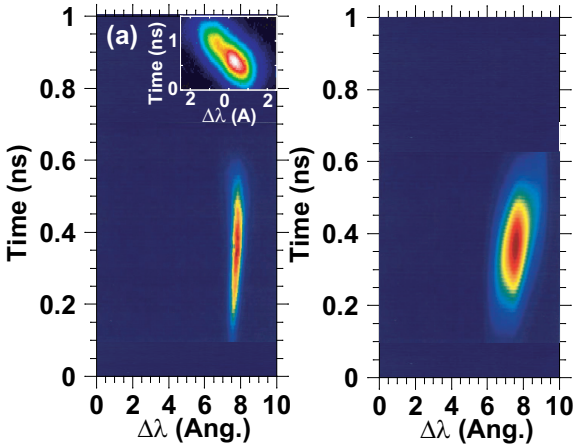

FIG. 3: (a) The narrow SBS spectra for a laser beam intensity of 1.7×10^{15} W-cm^{-2} indicates scattering from a uniform plasma created with a total heater beam energy of 16 kJ. At peak electron temperature ($T_e = 3.5$ keV), there is no measured SBS. Early in time, the plasma is cold ($T_e = 1.5$ keV) and a peak reflectivity of 25% is measured. The forward spectra is measured (insert) and shows a strong frequency shift in time. (b) The reflectivity is calculated using linear gains, Eq. 2. The wavelength shift early in time ($\Delta\lambda = 7.5$Å) is consistent with the simulated plasma parameters.

propagating through the target upto twice the original beam cone. The transmitted energy, spectrum, and temporal beam spray are measured. By correlating the plasma parameters, backscatter, and transmission measurements we are able to obtain a detailed scaling of reflectivity as a function of electron temperature.

Figure 2 shows a strong reduction in the backscattered light as the electron temperature along the hohlraum axis exceeds 2.5 keV for an interaction beam intensity of $I_p = 1.7 \times 10^{15}$ W-cm^{-2}. The decrease in reflectivity with increasing temperature is a direct result of reducing the SBS three wave coupling as evident in the linear gain for intensity,

$$G_{sbs} = 290 \cdot \lambda_o[\mu\text{m}] \left(\frac{n_e}{n_{cr}}\right) \left(\frac{L[\text{mm}]}{T_e[\text{keV}]}\right) \left(\frac{\omega_a}{\nu_a}\right) I_{15}[\text{W-cm}^{-2}] \qquad (1)$$

where $\frac{n_e}{n_{cr}} = 0.05$ is the fraction of electron density to the critical density for 3ω light, Z=2.2 is the average charge state for our fully ionized CH gas, and $L \sim 1.6$ mm is the gain length. T_e/T_i changes by less than 15% and the Landau damping for our conditions is $\nu_a/\omega_a \approx 0.3$. The theoretical curve in Fig. 2(a) is obtained by applying linear theory including pump

depletion [13] ,

$$R\,(1-R) = \epsilon e^{G_o \frac{T_o}{T_e}(1-R)} \tag{2}$$

where $\epsilon \approx 10^{-9}$ is the thermal noise. The peak linear SBS gain calculated by post processing the plasma properties from HYDRA simulations using the code LIP[14] is $G_o = 24$ for $T_o = 1.8$ keV. At this intensity ($I_p = 1.7 \times 10^{15}$ W-cm^{-2}) no backscattered light was detected by the NBI outside of the original beam cone. No SRS is measured in these experiments, as predicted by the moderate linear SRS gains ($G_{srs} < 20$).

The SBS spectra measured by FABS (Fig. 3a) for a power averaged intensity in the interaction beam of $I_p = 1.7 \times 10^{15}$ W-cm^{-2} shows a narrow feature that peaks when the interaction beam reaches maximum power and the plasma is cold ($T_e = 1.8$ keV). The temporal reflectivity and wavelength shift of this spectra are well reproduced by the linear gain calculations shown in Fig. 3b where the SBS power spectrum has been calculated using linear theory, Eq. 2. The simulated reflectivity is consistent with the measurements when the instrument function ($\sigma = 100$ ps) has been convolved to account for the time shear introduced by the spectrometer. Both the simulation and the experimental results show that when the plasma reaches a temperature above 2.5 keV, the total backscatter is less than 1%.

Furthermore, the simulated SBS frequency shift is consistent with the measured spectrum when accounting for the frequency change observed in the forward scattered light [15]. The frequency of the light propagating in the plasma is shifted as it moves through the changing density. This is observed by the 3ωTBD as the transmitted light is shifted by a few angstroms (Fig. 3) over the time of the experiment.

Low backscatter and high electron temperature leads to a peak transmission (Figure 4) greater than 90% for intensities $I_p \leq 2 \times 10^{15}$ W-cm^{-2}. The total scattered power (3ωTBD + backscatter) compares with well with HYDRA simulations that account for inverse bremsstrahlung absorbtion.

In addition to this high transmission, Fig. 5(b) shows that 75% of the total transmitted power is measured within the original ($f/6.7$) beam cone after propagation through the high temperature plasma. For intensities above $I_p > 2.0 \times 10^{15}$ W-cm^{-2}, transmission within twice the beam cone drops to 55% and 65% of the energy is outside of the original beam cone. Furthermore, backscattered light outside of the FABS is measured by the NBI. For the highest intensity shots (4×10^{15} W-cm^{-2}), 50% of the total backscattered energy is outside

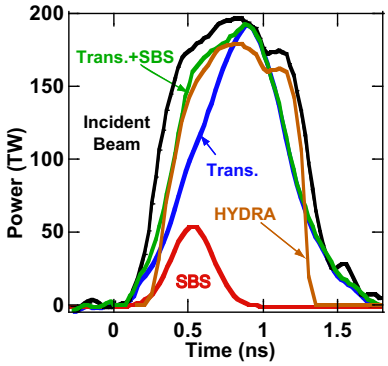

FIG. 4: At peak electron temperature (t=800 ps), we measure a peak transmission above 90% (blue curve) for an interaction beam intensity of $I_p = 1.4 \times 10^{15}$ W-cm^{-2}. The calculated transmission (orange curve) is determined by multiplying the absorption calculated by HYDRA with the incident laser pulse; these results compared to the total measured light in the interaction beam; the total measured light is equal to the sum of the measured transmission and the reflected light (red).

of the original beam cone.

Beam spray is a direct measure of filamentation; the filamentation threshold for an ideal beam can be calculated by balancing the plasma pressure with the pondermotive force resulting from the transverse profile of the laser beam [16]. Theoretical work using the laser-plasma interaction code Pf3D has extended this work to include the laser beam intensity profile with a random phase plate (RPP) [17],

$$FFOM = \frac{I_p \lambda^2}{10^{13}} \left(\frac{n_e}{n_{cr}}\right) \left(\frac{3}{T_e}\right) \left(\frac{f^{\#}}{8}\right)^2 \quad (3)$$

where I_p is the power averaged intensity at best focus, λ is the wavelength of the laser beam, $n_e/n_{cr} = 6\%$ is the fraction of electron density to the critical density at 3ω, $T_e = 3$ keV is the electron temperature, and $f^{\#} = 6.7$ is the ratio of the focal length to the beam diameter. When the filamentation figure of merit (FFOM) is greater than one, the beam is expected to experience significant filamentation and beam spray. Our measurements presented in Fig. 5(b) are compared with the peak FFOM determined by post-processing the parameters calculated by the hydrodynamic simulations where the filamentation threshold is calculated to be at $I_{FFOM} = 1.5 \times 10^{15}$ W-cm^{-2}; at intensities less than this threshold, there is good laser beam propagation through the plasma.

In summary, we have demonstrated laser beam propagation through ICF hohlraums at ignition plasma conditions. This is accomplished through high electron temperature plasmas

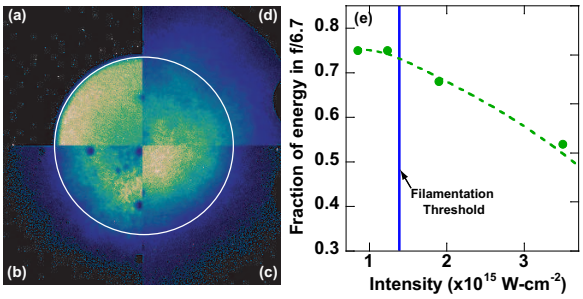

FIG. 5: The time integrated transmitted beam profile is a measure of the beam spray which is a direct indication of filamentation in the plasma; the incident intensity is varied (a) no plasma, (b) $I_p = 1.2 \times 10^{15}$W-cm^{-2}, (c) $I_p = 2 \times 10^{15}$W-cm^{-2}, (d) $I_p = 3.5 \times 10^{15}$W-cm^{-2}. (e) For intensities less than $I_{FFOM} = 1.5 \times 10^{15}$W-cm^{-2}, 70% of the energy is measured to remain in the original $f/6.7$ beam cone (circle).

that reduce the linear gains below their thresholds ($G_{sbs,srs} < 20$, FFOM< 1). For electron temperatures above 3 keV total backscatter is shown to be below 1% while producing a transparent plasma with a peak transmission greater than 90%. The laser beam is shown to propagate without beam spray for intensities below 2×10^{15} W-cm^{-2}; above this intensity the beam is shown to filament. These experiments verify the ability of current models to predict ignition hohlraum conditions and laser-plasma interaction linear gains for filamentation, SBS, and SRS. Furthermore, these results show the importance of predicting the electron temperature prior to peak power when the plasma is cold; a small change in the electron temperature can lead to a significant increase in the backscattered energy.

We would like to acknowledge the efforts of the Omega Laser Crew. This experiment was made possible by D. Hargrove, V. Rekow, J. Armstrong, K. Piston, R. Knight, S. Alverez, R. Griffith, and C. Sorce with their contributions to the 3ωTBD. We thank R. Wallace and his fabrication team for the excellent targets. This work was supported by LDRD 06-ERD-056 and performed under the auspices of the U.S. Department of Energy by the Lawrence Livermore National Laboratory under Contract No. W-7405-ENG-48 with University of California.

---

[1] J. D. Lindl *et al.*, Phys. Plasmas **11**, 339 (2004).

[2] W. L. Kruer, *The Physics of laser plasma interactions* (Addison-Wesley Publishing Company,

Inc., 1988).

[3] D. H. Froula *et al.*, Phys. Plasmas **13** (2006).

[4] J. M. Soures *et al.*, Laser Particle Beams **11**, 317 (1993).

[5] M. M. Marinak *et al.*, Phys. Plasmas **8**, 2275 (2001).

[6] S. H. Glenzer *et al.*, Phys. Plasmas **6**, 2117 (1999).

[7] A. J. MacKinnon *et al.*, Rev. Sci. Instrum. **75**, 3906 (2004).

[8] D. H. Froula *et al.*, Rev. Sci. Instrum. **In press** (2006).

[9] B. MacGowan *et al.*, Phys. Plasmas **3**, 2029 (1996).

[10] J. Moody *et al.*, Phys. Plasmas **7**, 3388 (2000).

[11] J. C. Fernandez *et al.*, Phys. Rev. Lett. **81**, 2252 (1998).

[12] B. H. Failor *et al.*, Physical Review E **59**, 6053 (1999).

[13] C. Tank, J. Appl. Phys. **37**, 2945 (1966).

[14] E. A. Williams, Report UCRL-LR-105820-98 (1998).

[15] T. DEWANDRE *et al.*, Phys. Fluids **24**, 528 (1981).

[16] P. KAW *et al.*, Phys. Fluids **16**, 1522 (1973).

[17] E. A. Williams, Phys. Plasmas **13**, 056310 (2006).